Journal of Materials Chemistry C

PAPER

View Article Online
View Journal | View Issue

Cite this: J. Mater. Chem. C, 2017, 5, 4480

Important role of ancillary ligand in the emission behaviours of blue-emitting heteroleptic Ir(III) complexes†

Yang-Jin Cho,[a] So-Yoen Kim,[a] Jin-Hyoung Kim,[a] Douglas W. Crandell,[b] Mu-Hyun Baik,*[bc] Jiwon Lee,[d] Chul Hoon Kim,[a] Ho-Jin Son,*[a] Won-Sik Han*[d] and Sang Ook Kang *[a]

Received 25th February 2017,
Accepted 10th April 2017

DOI: 10.1039/c7tc00844a

rsc.li/materials-c

A series of heteroleptic Ir(III) complexes composed of 2-(2,4-difluoro-3-(trifluoromethyl)phenyl)-4-methylpyridine ($dfCF_3$) as the main ligand and such ancillary ligands as acetylacetonate [$Ir(dfCF_3)_2(acac)$] (**acac**), picolinate [$Ir(dfCF_3)_2(pic)$] (**pic**), and tetrakis-pyrazolyl borate [$Ir(dfCF_3)_2(bor)$] (**bor**) were prepared, and their emission behaviors depending on the ancillary ligands were systematically investigated. It was found that the Huang–Rhys factors (S_Ms) of the emission decrease in the order **bor** (0.97) > **acac** (0.87) > **pic** (0.76), while the nonradiative rate constants ($k_{nr}/10^5$ s^{-1}) calculated from the quantum yields and lifetimes of emission were in the order **acac** (4.89) > **pic** (1.17) > **bor** (0.28). It was assumed that the large difference of k_{nr} for the complexes arose from important contributions of the ancillary ligands to the crossing from an emissive state (^{3}MLCT) to a nonemissive metal-centered state (^{3}MC). The activation energies for the crossing from ^{3}MLCT to ^{3}MC were estimated from the temperature dependencies of the emission lifetime and were found to be 46 meV for **acac**, 61 meV for **pic**, and >100 meV for **bor**. The experimental results were in line with the theoretical calculations based on integrating quantum chemical modeling methods. By the excellent emission behavior, **bor** was applied as a dopant to prototype deep-blue phosphorescent organic light-emitting diode devices, which revealed high emission efficiency and colour purity.

Introduction

Phosphorescent transition metal complexes are distinct from pure organic luminophores due to their characteristic long emission lifetimes, large absorption–emission Stokes shifts, and tunable excited states.[1,2] Transition metal complexes emit phosphorescence at room temperature due to the heavy atom effect that induces strong spin–orbit coupling (SOC), facilitating both fast intersystem crossing (ISC) from the excited singlet state to a triplet state and the spin-forbidden radiative process from the triplet state.[3,4] There are numerous reports on the photophysical and photochemical properties of transition metal complexes, particularly for Ru(II),[5,6] Ir(III),[7–10] and Pt(II) complexes.[11–13]

Among them, phosphorescent OLEDs based on cyclometalated Ir(III) emitters have exhibited high efficiencies with an external quantum efficiency (EQE) >20%.[14–19] However, stabilities of the various materials used in the OLED devices are key issues in the commercialization of phosphorescent OLEDs. Therefore, developing highly robust phosphorescent transition metal complexes is essential for their practical applications. In this regard, a primary requirement is that triplet emitters should be resistant to structural rearrangements as encountered in some Ir(III)-OLED emitters during thermal treatment[20,21] and should be stable against chemical degradation during operational device aging.[22,23] Indeed, the robustness of a phosphorescent metal complex is directly related to chemical changes, which are considered to occur, in many cases, by crossing from the phosphorescent state to a metal-centered d–d state.[24–26] In this state, an electron is populated in the metal–ligand (M–L) anti-bonding d_σ orbitals, and the electronic configuration associated with weakening of the M–L bond result in its rupture.[27] The crossing to a d–d state is believed to be a major non-radiative process.

The rate constant of non-radiative decay (k_{nr}) should provide an important measure for the crossing to a d–d state. It is

[a] Department of Advanced Materials Chemistry, Korea University, Sejong 30019, South Korea. E-mail: hjson@korea.ac.kr, sangok@korea.ac.kr
[b] Department of Chemistry, Indiana University, 800 E. Kirkwood Ave., Bloomington, IN 47405, USA
[c] Department of Chemistry, Korea Advanced Institute of Science and Technology (KAIST), Daejeon 34141, Republic of Korea. E-mail: mbaik2805@kaist.ac.kr
[d] Department of Chemistry, Seoul Women's University, Seoul 01797, South Korea. E-mail: wshan@swu.ac.kr

† Electronic supplementary information (ESI) available: Synthetic details, crystal data and collection parameters for **acac**, **pic** and **bor** and DFT results. CCDC 1518546 (**acac**), 1518551 (**pic**), 1518170 (**bor**). For ESI and crystallographic data in CIF or other electronic format see DOI: 10.1039/c7tc00844a

estimated from the phosphorescence quantum yield (Φ_P) and lifetime (τ_P): $\Phi_P = k_r \cdot \tau_P$ and $\tau_P = 1/(k_r + k_{nr})$; k_r = radiative rate constant. Therefore, one possible avenue to diminish k_{nr} is to design suitable ligands that can diminish excited-state structural distortions. Specifically, the so-called Huang–Rhys factor S serves to quantify the structural distortion ΔQ of the excited state on the ground state. If $S = 0$ (*i.e.* minimum ΔQ), the equilibrium geometries of the excited and ground states should be identical, and only a sharp peak corresponding to the 0–0 transition should be observed. With an increase of S (*i.e.* an increase of ΔQ) and hence an increase in S, vibronic progressions can be observed; the intensity ratios of the 0–0 and 0–1 vibrational peaks give $S : S = (I_{0-1}/I_{0-0})$. Since the overall emission bandwidth is associated with the vibronic progressions, a smaller S implies a spectrum of narrower bandwidth and higher colour purity of the emission.[28,29] Consequently, it is assumed that complexes with highly rigid scaffolds would be advantageous for developing highly luminescent materials. Since the magnitude of the Huang–Rhys factor is proportional to the square of the displacement in the excited state, the Huang–Rhys factor has frequently been used to estimate the degree of participation in a non-radiative process.[30] However, a more important factor that has been overlooked in this estimation is the activation barrier between the radiative triplet state (normally ^{3}MLCT and/or ^{3}LC) and a non-radiative state (usually ^{3}MC). Namely, even though the Huang–Rhys factor is small, the crossing to ^{3}MC would be facilitated if the activation energy is small. An opposite case can be true if the activation energy is large enough to suppress the crossing to ^{3}MC.

In this work, we report the excited-state behavior of a series of heteroleptic cyclometalated complexes composed of 2-(2,4-difluoro-3-(trifluoromethyl)phenyl)-4-methylpyridine as the main ligands and acetylacetonate (**acac**), picolinate (**pic**) and tetrakis-pyrazolyl borate (**bor**) as ancillary ligands. The synthesis and characterization of the complexes, as well as their photophysical and electrochemical properties, were systematically investigated. The effects of the different ancillary ligands on the excited-state behavior associated with the crossing to ^{3}MC are discussed in the results section. More precisely, its effects on photophysical properties are presented together with theoretical calculations. The developed heteroleptic Ir(III) complexes were tested as dopants in prototype phosphorescent organic light-emitting diode devices, and it was found that **bor** showed a deep-blue electro-luminescence with a high emission efficiency and colour purity.

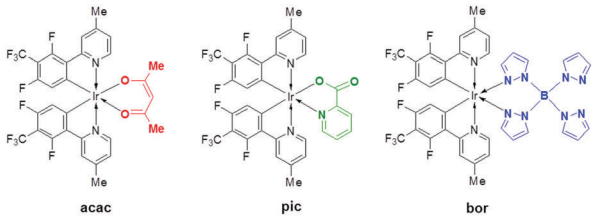

Chart 1 Chemical structures of heteroleptic Ir(III) complexes in this work.

The syntheses of all complexes were summarized in Scheme S1 (ESI†): Suzuki–Miyaura coupling between 2,4-difluorophenylboronic acid and 2-bromo-4-methylpyridine gave product 2-(2,4-difluorophenyl)-4-methylpyridine (**1**), which was transformed to the iodo derivative 2-(2,4-difluoro-3-iodophenyl)-4-methylpyridine (**2**) by treatment with lithium diisopropylamide (LDA) and iodine. Trifluoromethylation of (**2**) with copper(I) iodide in the presence of potassium fluoride and trifluoromethyl-trimethylsilane at room temperature for 24 hours afforded the cyclometalating ligand (**3**) in 20% yield. This ligand was used to prepare the cyclometalated, chloride-bridged diiridium(III)-complex, $[Ir(N\hat{}C)_2Cl]_2$ (N^C = 2-(2,4-difluoro-3-(trifluoromethyl)-phenyl)-4-methylpyridine) (**4**),[31] $IrCl_3 \cdot nH_2O$ and excess amounts of ligand (**3**) were dissolved in a 2-ethoxyethanol : H_2O (3 : 1) mixture and refluxed for 18 h. Finally, **acac** and **pic** were prepared according to a previously reported standard procedure,[32,33] in which the ligand exchange with corresponding ancillary ligands was successfully accomplished to yield the *bis*-cyclometalated Ir(III) complexes. **bor** was prepared by treating the cyclometalated, chloride-bridged diiridium(III)-complex with CF_3SO_3Ag to produce chloride-free, monometallic Ir-complex $(dfCF_3)_2Ir(H_2O)_2(CF_3SO_3)$, which was subsequently reacted with the potassium tetrakis(1-pyrazolyl)borate salt in acetonitrile solution to give the desired product in modest yields.[38]

The solid-state molecular structures of **acac**, **pic** and **bor** were determined by single-crystal X-ray diffraction using crystals grown in dichloromethane solution, as illustrated in Fig. 1. Details of the X-ray diffraction studies are given in Tables S1–S4 (ESI†). **acac**, **pic** and **bor** were fallen in the orthorhombic space group *Pccn*, a monoclinic space group $P2_1/c$ and a triclinic space group $P\bar{1}$ respectively. In all complexes, the iridium(III) center adopted a distorted octahedral coordination geometry with *cis*-metallated carbons and *trans*-pyridine nitrogen atoms. The N–Ir–N angles for the two *trans*-N,N atoms in **acac**, **pic** and **bor** were 175.28(17)°, 176.19(17)° and 175.19(19)°, respectively. Ir–C_{Ph} bond lengths

Results and discussion

Synthesis and crystal structures

All complexes depicted in Chart 1 were prepared under an inert gas atmosphere, isolated by flash column chromatography and were further purified by train sublimation in moderate yields. The formation of all compounds was confirmed by high-resolution mass spectrometry, elemental analysis and ^{1}H and ^{13}C NMR spectrometry. 2-(2,4-Difluorophenyl)-4-methylpyridine was prepared according to a previously reported method.[31]

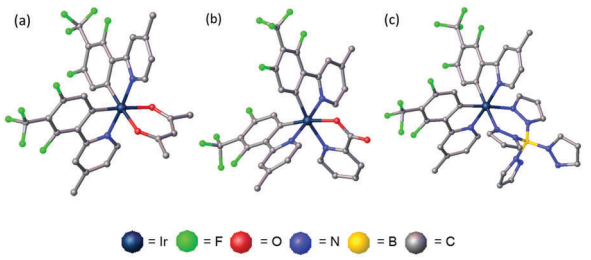

Fig. 1 Single crystal structures of **acac** (a), **pic** (b), and **bor** (c). Hydrogen atoms were omitted for clarity.

Table 1 Selected bond distances (Å) for **acac** (a), **pic** (b), and **bor** (c)

Bond distances (Å)					
acac		**pic**		**bor**	
Ir–C_{Ph}	1.971	Ir–C_{Ph}	1.983	Ir–C_{Ph}	2.002
Ir–C_{Ph}		Ir–C_{Ph}	2.006	Ir–C_{Ph}	2.008
Ir–N_{Py}	2.034	Ir–N_{Py}	2.038	Ir–N_{Py}	2.044
Ir–N_{Py}		Ir–N_{Py}	2.056	Ir–N_{Py}	2.059
Ir–O_{acac}	2.125	Ir–O_{pic}	2.139	Ir–N_{bor}	2.122
Ir–O_{acac}		Ir–N_{pic}	2.142	Ir–N_{bor}	2.169

of **acac** (1.971(3) Å), **pic** (2.006(5) and 1.983(5) Å) and **bor** (2.002(5) and 2.008(4) Å) were similar to the reported values for Ir(dfppy)$_2$(pic), Ir(tpy)$_2$(bor), and Ir(dfppy)$_2$(acac), respectively.[33–38] For heteroleptic compounds, the ancillary ligands were less tightly bound to the iridium(III) center compared to the main ligand, with **acac** (Ir–O: 2.125(3) Å), **pic** (Ir–N: 2.143(3) Å and Ir–O: 2.139(3) Å), **bor** (Ir–N: 2.122(4) and 2.169(5) Å) distances. The distances between the iridium centre and the coordinating atoms of the ancillary ligands **acac**, **pic** and **bor** were shown in Table 1. The distances between iridium and the main ligand (N^C) were the longest in **bor**. Within the series of compounds, the two phenyl–pyridine rings were roughly coplanar, but the dihedral angle showed that **pic** was the smallest with the value of 0.22°, followed by **acac** with the value of 1.46°, and **bor** was the most distorted with the value of 5.49°. These structural differences were expected to affect the photophysical properties of each compound as seen below.

Electrochemistry

The electrochemical properties of **acac**, **pic**, and **bor** were investigated by using cyclic voltammetry (CV), and their redox potentials were summarized in Table 2. CV was performed by utilizing a three-electrode cell system: platinum disk electrode was used as the working electrode, whereas a platinum wire and Ag/AgNO$_3$ were used as the counter and reference electrodes, respectively. All of the electrochemical data were measured relative to an internal ferrocenium/ferrocene reference (Fc^+/Fc). As shown in Fig. 2, the oxidation potentials of **acac**, **pic**, and **bor** were significantly different which showed oxidation at 0.90, 1.12, and 1.18 V, respectively. Increasing the ligand field strength of the ancillary ligand clearly leads to a higher oxidation potential which indicates ancillary ligands with stronger ligand field strength stabilize the HOMO (highest occupied molecular orbital) energy level. On the other hand, due to the limitation of the CV window, the reduction potentials of **acac** and **bor** were not obtained, while the reduction potential for **pic** was measured as −2.34 V, as shown in the Fig. 2 inset. Therefore, LUMO (lowest unoccupied molecular orbital) levels of **acac** and **bor** would be at higher energy level compare with **pic**.

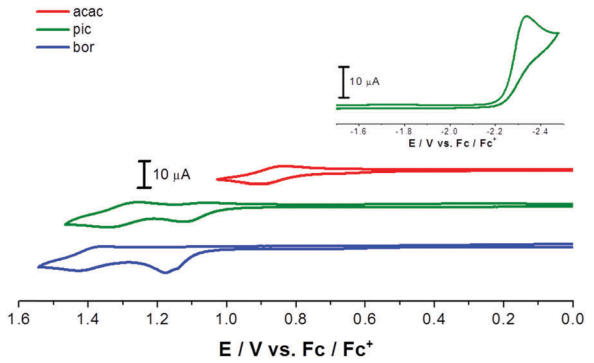

Fig. 2 Oxidation waves for 1 mM DCM solution of **acac**, **pic**, and **bor** containing 0.1 M TBAP taken at a scan rate of 0.1 V s^{-1} by cyclic voltammograms (inset: reduction wave of **pic**). Platinum disk electrode is the working electrode, and a platinum wire and Ag/AgNO$_3$ is the counter and reference electrodes, respectively.

Photophysical properties

Fig. 3 showed steady-state absorption spectra of the heteroleptic Ir(III)-complexes **acac**, **pic**, and **bor** in dichloromethane (DCM) solution. The absorption spectra at 298 K featured characteristic transitions that have been observed in other similar systems, and could tentatively be assigned to: (i) strong ligand-centered (LC) spin-allowed π → π* transitions between 243 and 264 nm and confirmed by absorption spectra of the ligand as shown in the Fig. S2 (ESI†), (ii) spin-allowed singlet metal to ligand charge transfer (^{1}MLCT) Ir-dπ → ppy-π* transitions between 320 and 380 nm, and (iii) a weak absorption band between 435 and 470 nm that was likely associated with a spin-forbidden ^{3}MLCT transition. In addition, even though it was not observed in absorption spectra, an energetically close-lying ligand-based excited state (^{3}LC) might be mixed together other states. As suggested and previously reported in the literature,[39] the lowest triplet excited state, T_1, would presumably be mixed in terms of orbital characteristics with a wave function description of $\Psi_{T1} = a\Psi_{3MLCT} + b\Psi_{3LC}$.

Table 2 Photophysical and electrochemical properties of the heteroleptic complexes

		Emission at 298 K					Emission at 77 K			
Complex	abs, λ_{max} λ (nm) [ε, 10^3 M^{-1} cm^{-1}][a]	λ (nm)	τ (μs)	Φ_{PL}	k_r (10^5 s^{-1})	k_{nr} (10^5 s^{-1})	λ (nm)	τ (μs)	E_{ox}/E_{red}[b] (eV)	HOMO[c]/ LUMO[d] (eV)
acac	246 (54.9), 263 (49.2), 323 (13.61), 379 (6.3), 416 (2.5), 446 (1.1)	470, 494	0.9	0.56	6.22	4.89	459, 491, 524	2.5	0.88/—	−5.68/−2.98
pic	260 (38.0), 279 (32.6), 372 (4.9), 448 (0.2)	455, 484	1.8	0.79	4.39	1.17	449, 481, 514	2.6	1.12/−2.33	−5.92/−3.16
bor	239 (6.8), 316 (11.4), 341 (6.8), 361 (5.4), 413 (0.4)	450, 478	4.6	0.87	1.89	0.28	446, 478, 510	4.9	1.18/—	−5.98/−3.19

[a] Measured in Ar-saturated DCM solution (10 μM) at 298 K. [b] Redox potentials were measured in DCM and their values are reported relative to Fc/Fc^+. [c] The HOMO level was determined using the following equation: E_{HOMO} (eV) = $-e(E_{ox} + 4.8)$. [d] The LUMO level was determined using the following equation: E_{LUMO} (eV) = $e(E_{HOMO} + E_g^{opt})$.

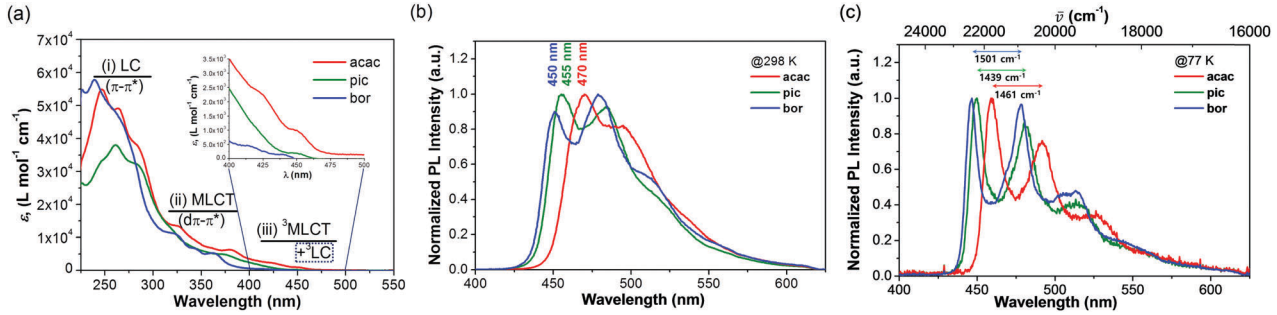

Fig. 3 (a) Steady-state absorption spectra for **acac**, **pic**, and **bor** in DCM solution at 298 K (inset: enlarged spectra from 400 to 500 nm). Emission spectra in DCM solution at 298 K (b) and mTHF solution at 77 K (c) for Ir(III) complexes.

The emission properties were investigated using steady-state photoluminescence spectroscopy at 298 K and 77 K, as shown in Fig. 3b and c, respectively. At 298 K, heteroleptic Ir(III) complexes exhibited different phosphorescence emission peaks with distinctive vibronic fine structures depending on the ancillary ligand at 470, 455, and 450 nm for **acac**, **pic**, and **bor**, respectively, which indicated that the emitting excited state was a mixed MLCT/LC state. At 77 K, **acac** exhibited two emission peaks at 459 and 492 nm, with vibronic progressions of 1461 cm^{-1}. **pic**, and **bor** showed similar phosphorescence emissions at 77 K with two emission peaks at 449 and 480 nm (vibronic progressions = 1439 cm^{-1}) for **pic** and two peaks at 446 and 478 nm (vibronic progressions = 1501 cm^{-1}) for **bor**. The vibronic mode at 1440–1500 cm^{-1} was known as the stretching vibration of the C_{ph}–C_{py} bond (A mode) of the main ligand, which increased in the order of **pic**, **acac** and **bor**. Table 3 shows the calculated dihedral angles for **acac**, **pic**, and **bor**, indicating that the dihedral angle of **bor** was the largest and **bor** was the most distorted. This suggested that the excited states of **acac**, **pic**, and **bor** may be affected by the distortion of the phenyl–pyridine. Furthermore, all Ir(III) complexes showed rigidochromic shift with a decrease in temperature from 298 K to 77 K. Therefore, spectral changes between 298 K and 77 K indicate that the emitting state involved a ^{3}MLCT state. In addition, the vibrational features became more defined at low temperature, as highlighted by a direct comparison of Fig. 3b and c. The vibrational fine structure observed in emission spectra was often the result of several overlapping satellites belonging to different vibronic transitions. Namely, cooling to 77 K resulted in more populated in ^{3}LC excited state as evidenced by the highly structured emission. Furthermore, it was reported that the intensity ratio of this first major vibrational transition to the highest energy peak (E_{em}(0–0)) was a measure of vibronic coupling between the ground and excited state (Huang–Rhys factor, S_M) and was proportional to the degree of structural distortion that occurs in the excited state relative to the ground state.[40] The dominant vibrational mode associated with the excited-state distortion (M) could be obtained from the energy difference (in cm^{-1}) of these vibronic transitions at 77 K, whereas the S_M value could be estimated from the peak heights. As shown by the energy curves in Fig. 4, the corresponding S_M values for **acac**, **pic**, and **bor** were 0.76, 0.87, and 0.97, respectively. This result indicated that the structure of **bor** in the excited state would be mostly changed, therefore, it was expected that its lifetime would be shortest among the series of Ir(III) complex in this work.

As shown in Fig. 5a for the emission decay profiles, the emission lifetime of **bor** (4.6 μs) at room temperature was however substantially longer than that of either **acac** (0.9 μs) or **pic** (1.8 μs) in dichloromethane solution. This was again true

Table 3 Calculated dihedral angles for **acac**, **pic**, and **bor**

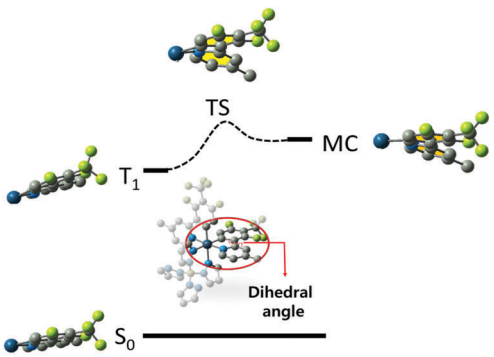

Dihedral angle (°)

	acac	pic	bor
S_0	0.63	0.07	1.77
T_1	2.17	0.28	2.01
TS	5.92	7.50	20.44
MC	8.53	8.23	16.26

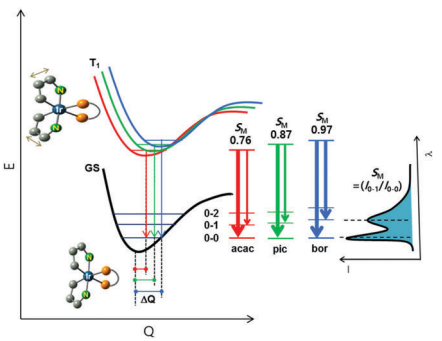

Fig. 4 Energy potential curves of **acac**, **pic** and **bor**.

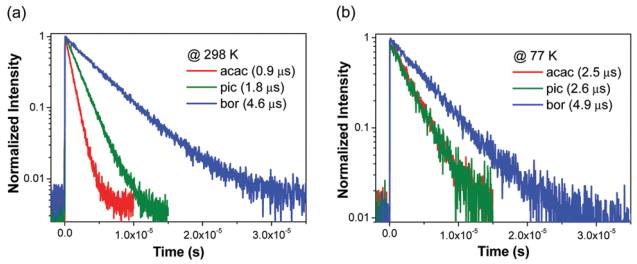

Fig. 5 Phosphorescence decay lifetime of Ir(III) complexes at 298 K in dichloromethane (a) and at 77 K in mTHF (b) with excitation at 355 nm.

even at 77 K as shown in Fig. 5b; the emission lifetime of **bor** (4.9 μs) was remarkably longer than that of **acac** (2.5 μs) or **pic** (2.6 μs). From the observed values of Φ_{em} and τ_{em}, the radiative (k_r) and nonradiative (k_{nr}) rate constants were calculated by using the following equations: $\tau_{rad} = \tau_{em}/\Phi_{em}$, $k_r = 1/\tau_{rad}$, $\Phi_{em} = k_r/(k_r + k_{nr})$, and $\tau_{em} = 1/(k_r + k_{nr})$. Therefore, there would be another factor that may determine the emission lifetime, such as an activation energy.

Mechanism of non-radiative decay

Fig. 6 conceptualized the most plausible non-radiative decay pathways expected for the ^{3}MLCT excited states of **acac**, **pic**, and **bor**. In heteroleptic complexes that carry an ancillary ligand with low lying π*-orbitals, two MLCT states must be considered: one in which the electron is excited into the cyclometalating ligand $\mathbf{L_1}$ and a second where the electron may be excited into the ancillary ligand $\mathbf{L_2}$. The ^{3}MLCT state responsible for phosphorescence was $\mathbf{T_1}$ and emerged from the singlet excited state **S*** by rapid intersystem crossing. It could decay back to the ground state $\mathbf{S_0}$ through a number of competitive radiative and non-radiative processes, which all contributed to the overall lifetime of the excited state. The non-radiative decay rate should be related to the energy gap law, as demonstrated in analogous Ru(II) and Os(II) complexes:[41,42] The non-radiative decay becomes more important when the energy gap between the emissive excited state and the ground state is increased by *e.g.* varying the ligand composition, as the radiative decay rate is inversely proportional to the energy gap. For the Ir complexes, the ^{3}MLCT state $\mathbf{T_1}$ formally consisted of a Ir(IV)–$(L)^{-1}$ fragment and the low-spin Ir(IV)-d^5 center necessarily has an asymmetrically occupied d–π orbitals among the t_{2g} orbitals of the pseudo-octahedral coordination environment. Therefore, these excited states were susceptible to first-order Jahn–Teller distortions along the vibrational vectors of the Ir–N bond stretching mode, which may lead to ligand dissociation. Due to the high oxidation state of Ir(IV) and the electron-richness of the photoreduced ligand, the M–L bond will likely cleave in a homolytic fashion, resulting in a five-coordinate, triplet Ir(III) complex. These intermediates were labeled $\mathbf{T_3}$ and $\mathbf{T_4}$ which emerged from $\mathbf{T_1}$ by traversing the bond cleavage transition states $\mathbf{TS_1}$ and $\mathbf{TS_2}$, as illustrated in Fig. 6. Rapid intersystem crossing to the singlet surface gave the metastable five-coordinate singlet state $\mathbf{S_1}$, which was a classical, coordinately unsaturated Ir(III)-low spin complex. Reattachment of the dangling ancillary ligand completed the reaction cycle and regenerated the reactant molecule $\mathbf{S_0}$ in what constituted a non-radiative decay of the $\mathbf{T_1}$ state.

The intersystem crossing from $\mathbf{T_3} \rightarrow \mathbf{S_1}$ and $\mathbf{T_4} \rightarrow \mathbf{S_2}$ was expected to be particularly efficient, as the spin–orbit coupling of the electrons so close to the Ir-center would be large and promote rapid electron spin interconversion.[3] Other temperature independent pathways for non-radiative decay, such as direct coupling between the triplet and ground states and vibrational coupling to the ground state,[43,44] were not explicitly considered in this work. Namely, this model plausibly suggested that the thermal accessibility of the metal-centered $\mathbf{T_3}$ and $\mathbf{T_4}$ states, governed by the activation barrier associated with $\mathbf{TS_1}$ and/or $\mathbf{TS_2}$, may be a major contributor to determining the lifetime of the emissive $\mathbf{T_1}$ intermediate.

For **pic**, the $\mathbf{T_2}$ state was 8.8 kcal mol^{-1} higher in energy than $\mathbf{T_1}$, which was not surprising, since the π*-orbital of the $dfCF_3$ ligand was much more delocalized and lower in energy compared to that of the ancillary ligand, picolinate. In addition, our calculations suggested that the non-radiative intermediate with picolinate ancillary ligand, $\mathbf{T_4}$, was 1.1 kcal mol^{-1} higher in energy than $\mathbf{T_1}$. This $\mathbf{T_4}$ state was thermodynamically more favorable than the $\mathbf{T_3}$ state which was a non-radiative intermediate with a main ligand. The kinetic barrier to reach $\mathbf{T_4}$ state from $\mathbf{T_1}$ state was only 2.9 kcal mol^{-1} which was substantially lower than the $\mathbf{T_3}$ state,

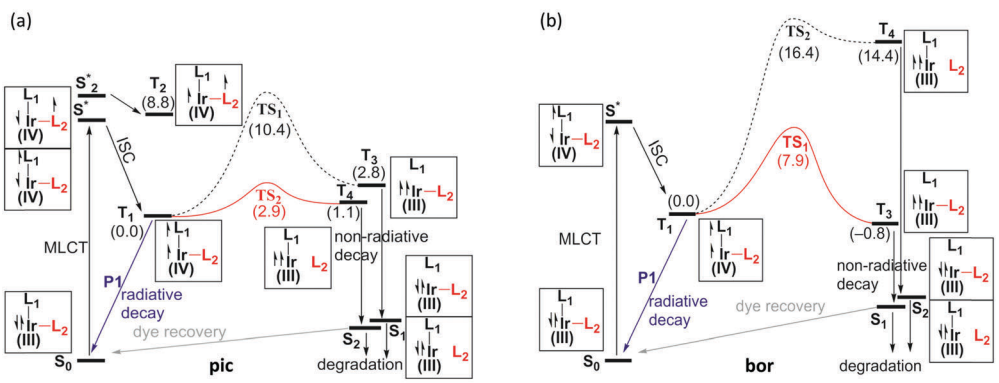

Fig. 6 Reaction profiles for Ir–N bond cleavage to form non-radiative $\mathbf{T_3}$ and $\mathbf{T_4}$ states for heteroleptic complexes (a) **pic** and (b) **bor** (reaction profile **acac** and explanations are in ESI,† Fig. S5).

10.4 kcal mol^{-1}. This finding was alarming, as it suggested that employing picolinate as an ancillary ligand was counter-productive and did not enhance the photoluminescence of the Ir-complex. We found that **acac** displayed a very similar behavior. The computed reaction profiles and supplemental discussions are given in the ESI.†

The detrimental impact of the picolinate ligand on the stability of the ^{3}MLCT state raises the question whether the opposite effect can be engineered by employing an ancillary ligand that cannot access a $\mathbf{T_4}$ state. The computed reaction energy profiles for **bor** are shown in Fig. 6b. Interestingly, the $\mathbf{T_3}$ state was found to be 0.8 kcal mol^{-1} lower in energy with respect to the $\mathbf{T_1}$ state, but the activation energy required to reach the $\mathbf{T_3}$ state was dramatically increased to 7.9 kcal mol^{-1}. In addition to the aforementioned electronic effect, the steric demands of the borate ligand made reorganization into the trigonal bipyramidal geometry of $\mathbf{T_3}$ difficult. The bulkiness of the borate ligand also contributed to a $\mathbf{T_4}$ state that was 14.4 kcal mol^{-1} higher in energy than the $\mathbf{T_1}$ state as the pyrazolyl moiety was unable to rotate away from the Ir center. The pyrazolyl fragments of the anionic borate ligand did not possess any low-lying vacant π*-orbitals and consequently the ancillary ligand could not participate in the MLCT process to generate a $\mathbf{T_2}$ state as was the case for **pic**. Even though the calculated absolute values could be different compared with the experimental values, we believed that the trends of the calculated results could support the experimental data.

Temperature dependent emission properties

To support our hypothesis, we investigated temperature dependent emission properties of **acac**, **pic**, and **bor**. Fig. 7 showed the evolution of intrinsic deactivation rate constant (k_{in}) as a function of temperature from 293 to 343 K. **acac** clearly showed a reduced emission lifetime at a higher temperature, while **bor** showed an almost invariant emission lifetime at different temperatures. This indicated that the activation energy from T_1 to the ^{3}MC for **bor**, was much higher than for **acac**. The activation energies of each one of the complexes were estimated by using the intrinsic deactivation rate constant, $k_{in}(T) = 1/\tau(T)$ where τ was the excited-state lifetime at a certain temperature T which could be estimated by the following equation:[45–47]

$$1/\tau(T) = k_0 + A_1 \exp(-\Delta E_1/k_B T) + A_2 \exp(-\Delta E_2/k_B T)$$

In this equation, k_0 was a temperature independent term, and the second and third terms contained frequency factors (A_1 and A_2) with activation energy barriers (ΔE_1 and ΔE_2) which could be expressed by an Arrhenius-type equation. The second term represented thermal redistribution between the triplet sublevels which depended on the zero field splitting (zfs). Since this second term could be treated as a constant above 293 K and the first term was the temperature-independent term as indicated above, the third term which represented the thermal population of non-radiative ^{3}MC state played a predominant role to determining activation energy barriers of **acac**, **pic**, and **bor**. The estimated activation energies for **acac** and **pic** were 46 and 61 meV, respectively. The activation energy for **bor** could not be assumed but it could be assumed to be higher than 100 meV. Therefore, when combining the quantum chemical modelling method and temperature dependent emission lifetime measurements, we could conclude that the activation energy from T_1 to ^{3}MC could be controlled by using different ancillary ligand in Ir(III) heteroleptic complexes.

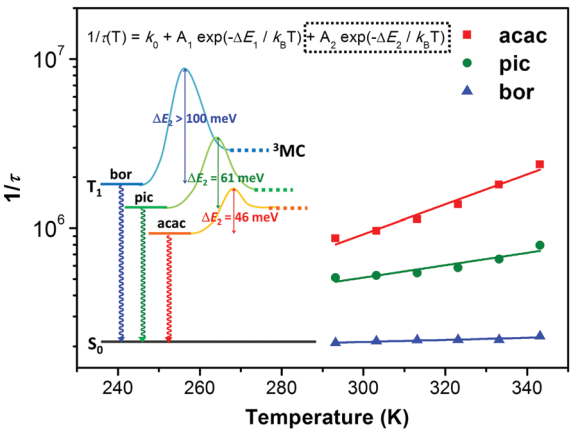

Fig. 7 Temperature-dependent excited-state deactivation rates ($k_{in} = 1/\tau$) of **acac**, **pic**, and **bor**. Excited-state lifetimes were determined from the luminescence decays with the time-correlated single photon counting technique.

Device performance

The blue phosphorescent OLED device was fabricated using **pic** and **bor** as dopants with the following device structure: ITO/HAT-CN (10 nm)/TAPC (85 nm)/mCBP:**bor** or **pic** (30 nm, 8 wt%)/TmPyPB (30 nm)/Liq (1 nm)/Al (150 nm) where HAT-CN stood for 1,4,5,8,9,11-hexaazatriphenylene-hexacarbonitrile, TAPC 4,4′-cyclohexylidene-bis[*N*,*N*-bis(4-methylphenyl)benzeneamine], and TmPyPB 1,3,5-tri(*m*-pyridin-3-ylphenyl)benzene. HAT-CN was used as the hole injection layer (HIL) material with a deep-lying lowest unoccupied molecular orbital (LUMO) to reduce the driving voltage and improve voltage stability and power efficiencies.[48–50] The triplet energy levels of TAPC (2.87 eV), mCBP (2.90 eV), and TmPyPB (2.80 eV) were higher than those of **pic** and **bor**; thus, effective confinement of the triplet excitons within the emission layer was expected. Fig. 8 and Table 4 showed the device characteristics. Blue emitting heteroleptic Ir(III) complexes were employed as triplet-emitting dopants. Among the heteroleptic Ir(III) complexes, **bor** outperformed over other heteroleptic Ir(III) complexes, **acac** or **pic** achieving the highest blue emission (**acac**: 459 nm, **pic**: 449 nm and **bor**: 446 nm) and recording a high Q.Y. (**acac**: 56% < **pic**: 79% < **bor**: 87%). The unique properties of **bor** have also been observed in the devices consistent to our understanding of its inherent HOMO energy. Triplet energy confinement of **bor** by the common layer materials provides a high current efficiency of 32.9 cd A^{-1}, which corresponds to an external quantum efficiency of 21.5%. The **bor** device exhibited lower turn-on voltage at 3.7 V with a maximum power efficiency up to 25.4 lm W^{-1} superior to **acac** (4.6 V) or **pic** (4.0 V), whereas the Commission Internationale d'Echairage (CIE) coordinates value [0.14, 0.20] was slightly higher than that of

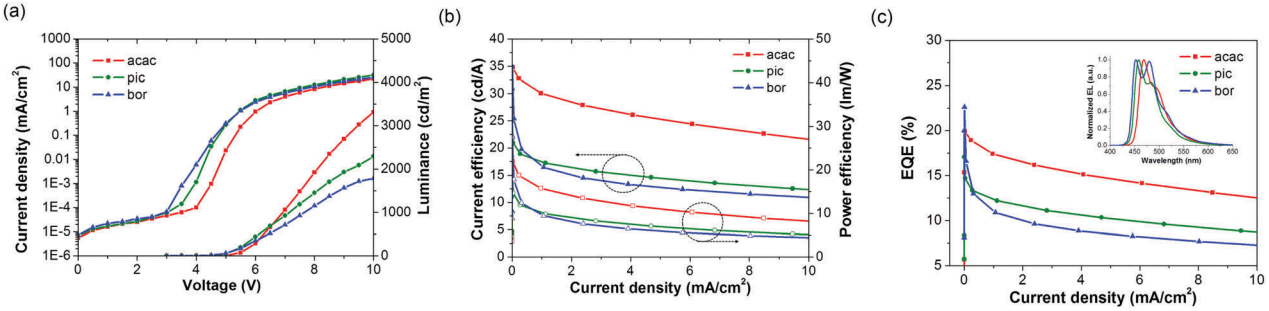

Fig. 8 Performances of devices **acac**, **pic** and **bor** (a) *J*–*V*–*L* characteristics and (b) current efficiency–current density–power efficiency (c) external quantum efficiency and EL spectra for devices **acac**, **pic** and **bor**.

Table 4 Device structure and characteristics of the PHOLEDs using **acac**, **pic** or **bor** as dopants

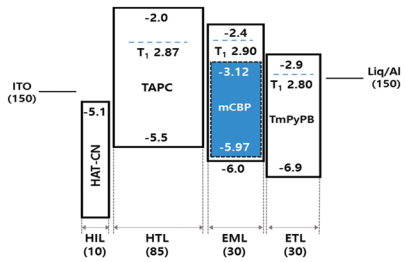

	Max current efficiency (cd A^{-1})	Max power efficiency (lm W^{-1})	Turn-on voltage (V)	CIE (*x*, *y*)	Max EQE (%)
acac	34.8	21.9	4.6	(0.14, 0.26)	19.9
pic	22.5	16.4	4.0	(0.14, 0.18)	15.5
bor	32.9	25.4	3.7	(0.14, 0.20)	22.6

Device structure: [ITO (150 nm)/HAT-CN (10 nm)/TAPC (85 nm)/mCBP: **acac**, **pic** or **bor** (30 nm, 8 wt%)/TmPyPB (30 nm)/Liq/Al (150 nm)].

pic [0.14, 0.18] and the roll-off phenomenon was prominently accelerated. A notable difference on the device performance may be arisen due to the HOMO energies of the dopants. In particular, the HOMO energy of **bor** was low enough to get closer to that of the host, mCBP; there seemed to be hardly any trap sites in **bor** resulting in a low turn-on voltage. However, this in turn gives rise to an adverse effect in the efficiency measurements in Fig. 8b because a p-type host, mCBP, required to have a certain amounts of trap sites to achieve charge valance for higher device performance. In additions, as shown below, the EL spectra are almost similar to the PL spectra of the dopants, suggesting that the energy transfer from mCBP to the dopant is well facilitated. These data are now updated in the ESI† (see Fig. S5).

Conclusions

In this work, a series of heteroleptic Ir(III) complexes, **acac**, **pic**, and **bor**, were prepared and their electrochemical and photophysical properties as well as different activation energies depending on ancillary ligand were systematically investigated. Even though the Huang–Rhys factors indicate the structure of **bor** in the excited state would be mostly changed, result shows that the emission lifetime of **bor** is longest among the series. We carried out theoretical quantum chemical calculations and measured experimental temperature dependent emission lifetime to explain the importance of activation energy barriers from T_1 state to ^{3}MC state in heteroleptic Ir(III) complexes. As a result, both theoretical and experimental investigations showed that the activation energy barrier for **bor** is significantly higher than **acac** and **pic**, which was estimated by temperature dependent emission lifetime experiments with the values of 46, 61, and higher than 100 meV, respectively. Therefore, we can conclude and proved that the activation energy from T_1 to ^{3}MC can be controlled by using different ancillary ligand in Ir(III) heteroleptic complexes. Finally, based blue phosphorescent OLED device was fabricated and the device shows a high current efficiency of 32.9 cd A^{-1}, which corresponds to an external quantum efficiency of 21.5%.

Acknowledgements

This work was supported by the MOTIE Ministry of Trade, Industry & Energy (10051379) and KDRC (Korea Display Research Corporation) support program for the development of future devices technology for display industry, the International Science and Business Belt Program through the Ministry of Science, ICT and Future Planning (2015K000287), the Basic Science Research Program through the National Research Foundation of Korea (NRF) funded by the Ministry of Education (NRF-2014R1A6A1030732).

Notes and references

1 N. D. McClenaghan, Y. Leydet, B. Maubert, M. T. Indelli and S. Campagna, *Coord. Chem. Rev.*, 2005, **249**, 1336.
2 Q. Zhao, S. Liu, M. Shi, C. Wang, M. Yu, L. Li, F. Li, T. Li and C. Huang, *Inorg. Chem.*, 2006, **45**, 6152.
3 H. Yersin, A. F. Rausch, R. Czerwieniec, T. Hofbeck and T. Fischer, *Coord. Chem. Rev.*, 2011, **255**, 2622.
4 H. Yersin, *Highly Efficient OLEDs with Phosphorescent Materials*, Wiley-VCH, Weinheim, 2008.

5 D. P. Rillema, D. G. Taghdiri, D. S. Jones, L. A. Worl, T. J. Meyer, H. A. Levy and C. D. Keller, *Inorg. Chem.*, 1987, **26**, 578.
6 B. J. Coe, D. W. Thompson, C. T. Culbertson, J. R. Schoonover and T. J. Meyer, *Inorg. Chem.*, 1995, **34**, 3385.
7 S. Lamansky, P. Djurovich, D. Murphy, F. Abdel-Razzaq, H. E. Lee, C. Adachi, P. E. Burrows, S. R. Forrest and M. E. Thompson, *J. Am. Chem. Soc.*, 2001, **123**, 4304.
8 F. Neve, M. La Deda, A. Crispini, A. Bellusci, F. Puntoriero and S. Campagna, *Organometallics*, 2004, **23**, 5856.
9 K. Dedeian, J. Shi, N. Shepherd, E. Forsythe and D. C. Morton, *Inorg. Chem.*, 2005, **44**, 4447.
10 R. Ragni, E. A. Plummer, K. Brunner, J. W. Hofstraat, F. Babudri, G. M. Farinola, F. Naso and L. D. Cola, *J. Mater. Chem.*, 2006, **16**, 1161.
11 K. P. Balashev, M. V. Puzyk, V. S. Kotlyar and M. V. Kulikova, *Coord. Chem. Rev.*, 1997, **159**, 109.
12 J. G. Williams, S. Develay, D. L. Rochester and L. Murphy, *Coord. Chem. Rev.*, 2008, **252**, 2596.
13 Z. He, W. Y. Wong, X. Yu, H. S. Kwok and Z. Lin, *Inorg. Chem.*, 2006, **45**, 10922.
14 L. Xiao, S. J. Su, Y. Agata, H. Lan and J. Kido, *Adv. Mater.*, 2009, **21**, 1271.
15 H. Sasabe, E. Gonmori, T. Chiba, Y. J. Li, D. Tanaka, S. J. Su, T. Takeda, Y. J. Pu, K. I. Nakayama and J. Kido, *Chem. Mater.*, 2008, **20**, 5951.
16 K. Udagawa, H. Sasabe, F. Igarashi and J. Kido, *Adv. Opt. Mater.*, 2016, **4**, 86.
17 S. J. Su, E. Gonmori, H. Sasabe and J. Kido, *Adv. Mater.*, 2008, **20**, 4189.
18 Y. Seino, H. Sasabe, Y. J. Pu and J. Kido, *Adv. Mater.*, 2014, **26**, 1612.
19 J. Lee, H.-F. Chen, T. Batagoda, C. Coburn, P. I. Djurovich, M. E. Thompson and S. R. Forrest, *Nat. Mater.*, 2016, **15**, 92.
20 J. M. Fernández-Hernández, C. H. Yang, J. I. Beltrán, V. Lemaur, F. Polo, R. Fröhlich, J. Cornil and L. De Cola, *J. Am. Chem. Soc.*, 2011, **133**, 10543.
21 E. Baranoff, S. Suàrez, P. Bugnon, C. Barolo, R. Buscaino, R. Scopelliti, L. Zuppiroli, M. Graetzel and M. K. Nazeeruddin, *Inorg. Chem.*, 2008, **47**, 6575.
22 S. Schmidbauer, A. Hohenleutner and B. König, *Adv. Mater.*, 2013, **25**, 2114.
23 Y. Zheng, A. S. Batsanov, R. M. Edkins, A. Beeby and M. R. Bryce, *Inorg. Chem.*, 2012, **51**, 290.
24 T. Sajoto, P. I. Djurovich, A. B. Tamayo, J. Oxgaard, W. A. Goddard and M. E. Thompson, *J. Am. Chem. Soc.*, 2009, **131**, 9813.
25 J. F. Riehl, Y. Jean, O. Eisenstein and M. Pelissier, *Organometallics*, 1992, **11**, 729.
26 L. Yang, F. Okuda, K. Kobayashi, K. Nozaki, Y. Tanabe, Y. Ishii and M.-A. Haga, *Inorg. Chem.*, 2008, **47**, 7154.
27 K. Li, S. M. Tong, Q. Wan, G. Cheng, W. Y. Tong, W. H. Ang, W. L. Kwong and C. M. Che, *Chem. Sci.*, 2016, **7**, 1653.
28 M. D. Jong, L. Seijo, A. Meijerinka and F. T. Rabouwa, *Phys. Chem. Chem. Phys.*, 2015, **17**, 16959.
29 D. W. Cooke, B. L. Bennett, K. J. McClellan, J. M. Roper and M. T. Whittaker, *J. Appl. Phys.*, 2000, **87**, 7793.
30 A. F. Rausch, L. Murphy, J. A. G. Williams and H. Yersin, *Inorg. Chem.*, 2012, **51**, 312.
31 H. J. Park, J. N. Kim, H. J. Yoo, K. R. Wee, S. O. Kang, D. W. Cho and U. C. Yoon, *J. Org. Chem.*, 2013, **78**, 8054.
32 M. A. Baldo, D. F. O'Brien, Y. You, A. Shoustikov, S. Sibley, M. E. Thompson and S. R. Forrest, *Nature*, 1998, **395**, 151.
33 J. Li, P. I. Djurovich, B. D. Alleyne, M. Yousufuddin, N. N. Ho, J. C. Thomas, J. C. Peters, R. Bau and M. E. Thompson, *Inorg. Chem.*, 2005, **44**, 1713.
34 A. B. Tamayo, B. D. Alleyne, P. I. Djurovich, S. Lamansky, I. Tsyba, N. N. Ho, R. Bau and M. E. Thompson, *J. Am. Chem. Soc.*, 2003, **125**, 7377.
35 S. Lamansky, P. Djurovich, D. Murphy, F. Abdel-Razzaq, R. Kwong, I. Tsyba, M. Bortz, B. Mui, R. Bau and M. E. Thompson, *Inorg. Chem.*, 2001, **40**, 1704.
36 E. Baranoff, B. F. Curchod, J. Frey, R. Scopelliti, F. Kessler, I. Tavernelli, U. Rothlisberger, M. Graetzel and M. K. Nazeeruddin, *Inorg. Chem.*, 2012, **51**, 215.
37 E. Baranoff, B. F. Curchod, F. Monti, F. Steimer, G. Accorsi, I. Tavernelli, U. Rothlisberger, R. Scopelliti, M. Graetzel and M. K. Nazeeruddin, *Inorg. Chem.*, 2012, **51**, 799.
38 J. Li, P. I. Djurovich, B. D. Alleyne, I. Tsyba, N. N. Ho, R. Bau and M. E. Thompson, *Polyhedron*, 2004, **23**, 419.
39 K. P. Zanoni, B. K. Kariyazaki, A. Ito, M. K. Brennaman, T. J. Meyer and N. Y. Murakami Iha, *Inorg. Chem.*, 2014, **53**, 4089.
40 C. E. McCusker and J. K. McCusker, *Inorg. Chem.*, 2011, **50**, 1656.
41 J. V. Caspar, E. M. Kober, B. P. Sullivan and T. J. Meyer, *J. Am. Chem. Soc.*, 1982, **104**, 630.
42 E. M. Kober, J. V. Caspar, R. S. Lumpkin and T. J. Meyer, *J. Phys. Chem.*, 1986, **90**, 3722.
43 K. F. Freed and J. Jortner, *J. Chem. Phys.*, 1970, **52**, 6272.
44 R. Englman and J. Jortner, *Mol. Phys.*, 1970, **18**, 145.
45 J. V. Caspar and T. J. Meyer, *J. Am. Chem. Soc.*, 1983, **105**, 5583.
46 R. D. Costa, F. Monti, G. Accorsi, A. Barbieri, H. J. Bolink, E. Ortí and N. Armaroli, *Inorg. Chem.*, 2011, **50**, 7229.
47 J. V. Houten and R. J. Watts, *J. Am. Chem. Soc.*, 1976, **98**, 4853.
48 M. Y. Chan, S. L. Lai, K. M. Lau, M. K. Fung, C. S. Lee and S. T. Lee, *Adv. Funct. Mater.*, 2007, **17**, 2509.
49 L. S. Liao, W. K. Slusarek, T. K. Hatwar, M. L. Ricks and D. L. Comfort, *Adv. Mater.*, 2008, **20**, 324.
50 L. S. Liao and K. P. Klubek, *Appl. Phys. Lett.*, 2008, **92**, 223311.